First-principles, general-potential local-orbital calculations for bulk crystals

Steven C. Erwin, Mark R. Pederson, and Warren E. Pickett
Complex Systems Theory Branch, Condensed Matter and Radiation Sciences Division, Naval Research Laboratory, Washington, D.C. 20375-5000
(Received 28 December 1989)

We describe a first-principles computational technique for calculating electronic structure, using the method of linear combination of atomic orbitals (LCAO). Gaussian-type orbitals are used, so that all matrix element integrals are calculated analytically. The technique makes no shape approximations to either the charge density or the effective one-electron potential, aside from the usual local-density approximation to the exchange-correlation potential. We have applied the method to three qualitatively different systems: diamond, vanadium, and a diamond-nickel (001) ideal interface supercell. To assess the accuracy of this technique, we have performed parallel calculations using the linear augmented-plane-wave (LAPW) method. In this way, all possible discrepancies due to choice of lattice constant and exchange-correlation potential are removed. Detailed comparisons between the LCAO and LAPW results for all three systems are made. Overall agreement between the two methods is excellent.

I. INTRODUCTION

Accurate solution of the Kohn-Sham equations is a central requirement for most first-principles electronic-structure calculations of the solid state. This need has spawned, in the last two decades, a variety of computational techniques that serve different computing objectives. While empirical and semiempirical approaches continue to be of interest, the majority of effort in recent years has centered on first-principles methods, which require no experimental information other than atomic numbers and positions of the basis atoms in the unit cell. Equally important has been the emphasis on self-consistent approaches, which of necessity impose no restrictions on the Coulomb potential other than translational invariance and the local site symmetry appropriate to a particular system.

The techniques that meet these requirements and currently find the widest application may be divided into two camps: reciprocal-space techniques (e.g., plane-wave basis) and real-space techniques (e.g., local basis). Each approach has its advantages and disadvantages. Since our research interests require accurate (first-principles) calculations on potentially very large supercells, we are particularly interested in methods that use small, efficient basis sets. Equally important is the *scaling* of the computational cost with the number of atoms per unit cell, N. It is well known[1] that for large N, the computational bottleneck for **k**-space methods is the setup and diagonalization of the Hamiltonian, which may in some cases account for as much as 95% of the entire iteration cycle for a plane-wave basis, and 75% for an augmented-plane-wave basis. Furthermore, because the basis functions are essentially of infinite extent, this time requirement scales with N^3, effectively creating a computational barrier to progress on much larger unit cells. Partly for this reason, algorithms that avoid this N^3 scaling, e.g., Car-Parrinello approaches,[2] are finding increasing application to **k**-space methods.

With a local-orbital basis, however, this computational burden is significantly alleviated in three ways. First, for calculations of comparable accuracy, the local-orbital basis-set size is typically from 2 to 5 times smaller than for the plane-wave basis. As a result, the diagonalization step time requirement is a much smaller fraction of the total time. Second, local-orbital Hamiltonian setup times are not characterized by the N^3 scaling described above. Since the basis functions are localized, contributions to a given matrix element from atoms far away are negligible. Furthermore, only matrix elements between nearby basis functions needed be retained, so that the resulting Hamiltonian is diagonally dominant. Consequently, for very large N the Hamiltonian setup time essentially scales with N. Finally, such sparse matrices may be diagonalized by specialized methods characterized by scaling laws more favorable than N^3.

In light of our future research needs, the above considerations have led us to develop an accurate, first-principles, local-orbital electronic-structure code. We have chosen to use the linear combination of atomic orbitals (LCAO) framework and a Gaussian-orbital basis set. In addition to the favorable scaling, the LCAO method enjoys a number of other advantages. It provides a "natural" basis set, in the sense that most crystalline systems resemble, to a considerable degree, a collection of atoms. As a result, the physical interpretation of eigenvectors in the LCAO basis is relatively straightforward, so that analysis of bonding and charge transfer effects is also simplified. By supplementing the (contracted Gaussian) atomic basis with (uncontracted) single Gaussian functions, even strongly covalent materials can be accurately described.

An important requirement for any new computational technique is that it reproduce results obtainable by well-established methods. We demonstrate this by carrying out parallel calculations using both the LCAO method

and the general-potential linear augmented-plane-wave (LAPW) method of Andersen,[3] as implemented by Krakauer and collaborators.[4] By using the same lattice constant and exchange-correlation potential, we can unambiguously eliminate discrepancies between the two results that might be due to these choices. The resulting comparison, which we present in Sec. III, thus provides a stringent test of our LCAO method.

The remainder of this paper is organized as follows. In Sec. II, we describe in detail our version of the LCAO method. Section III consists of the parallel application of our LCAO and the LAPW method to three test cases: an insulator (diamond), a transition metal (vanadium), and a supercell that we have recently used[5,6] to model the diamond-nickel (001) interface. We show that the LCAO and LAPW results for all three cases are in excellent agreement. In Sec. IV we provide some concluding remarks.

II. DETAILS OF THE LCAO METHOD

The LCAO method has a substantial history,[7] and so we restrict ourselves here to a summary of the most important details. Basis functions are chosen to be **k** dependent, phased lattice sums of both contracted and single Gaussian orbitals:

$$b_{\gamma j}(\mathbf{k},\mathbf{r})=N^{-1/2}\sum_{\nu}\exp[i\mathbf{k}\cdot(\mathbf{R}_\nu+\mathbf{T}_\gamma)] \times\phi_{\gamma j}(\mathbf{r}-\mathbf{R}_\nu-\mathbf{T}_\gamma)\ . \quad (1)$$

In the above, γ labels the atom found at position $\mathbf{T}_\gamma$ within the unit cell, j labels the atomic orbital, and the $\mathbf{R}_\nu$ are the Bravais-lattice vectors. The functions $\phi(\mathbf{r})$ are expanded on a set of Gaussian orbitals,

$$\phi(\mathbf{r})=\sum_m c_m\exp(-g_m r^2) \quad (2)$$

in which the number of terms is either 1 (for a single Gaussian function) or of order 10–20 (for a contracted function representing an atomic orbital). Equation (2) applies only to s-like states; for states of p or d symmetry, the appropriate angular factor is included in the definition.

With the basis functions defined this way, all the overlap matrix elements can be calculated analytically.[8] If one can also express the effective (Coulomb plus exchange correlation) potential $V_{\rm eff}(\mathbf{r})$ as a superposition of Gaussian-type functions, then all matrix elements of the Hamiltonian can also be calculated analytically or in terms of the error function. We find a Gaussian representation for this potential by first tabulating $V_{\rm eff}(\mathbf{r})$ on a dense mesh, then performing a least-squares fit:

$$V_{\rm eff}(\mathbf{r})\approx\sum_{i,j,\nu} d_{ij}h_{ij}(\mathbf{r}-\mathbf{R}_\nu-\mathbf{S}_j)\ . \quad (3)$$

We choose the fitting functions $h_{ij}(\mathbf{r})$ to have the form $h(\mathbf{r})=r^p\exp(-\omega r^2)$. The exponent p is given the value -1 or 0, corresponding to the nuclear or electronic contribution to the potential, respectively. There are no restrictions on the fitting function centers $\mathbf{S}_j$, and although they are always chosen to include the atom positions $\mathbf{T}_\gamma$, it is often useful to choose additional sites corresponding to approximate bond "centers." For the case $p=-1$ and $\mathbf{S}_j=\mathbf{T}_\gamma$, the corresponding fit coefficient is constrained to have the value $-Z_\gamma$, which in effect removes the nuclear potential spike prior to fitting the electronic contribution. Although angular factors conforming to the local point-group symmetry may also be appended to the definition of the fitting functions, in practice we use only spherical functions in the interest of simplicity. Note, however, that a superposition of spherical functions automatically produces nonspherical angular dependence at every point for which the overlap is nonzero. The above procedure is computationally simple, and has the advantage that the fitting error is easy to monitor. By using from 10 to 20 fitting functions per atom, and a single function between nearest-neighbor pairs of atoms, we have always been able to limit the rms fit error to 0.1 eV. For matrix elements between states with appreciable spatial extent, contributions to the integral are from a region that includes several oscillations in the fit error, giving a matrix element error that is substantially less than the rms fit error.

In order to calculate and tabulate the effective potential $V_{\rm eff}(\mathbf{r})$, an accurate and efficient method is needed for calculating the electronic contribution to the Coulomb potential. We use a combination of cubic spline[9] and fast Fourier transform integration techniques that meets both of these requirements. One begins by writing the total crystal charge density as a sum of localized (L) and nonlocalized (NL) electronic contributions, plus the nuclear charges:

$$\rho^{\rm crys}(\mathbf{r})=\rho_{\rm L}^{\rm crys}(\mathbf{r})+\rho_{\rm NL}^{\rm crys}(\mathbf{r})+\rho_{\rm nuc}^{\rm crys}(\mathbf{r})\ . \quad (4)$$

The decomposition of electronic density into localized and nonlocalized pieces is, of course, arbitrary. By judicious choice of $\rho_{\rm L}^{\rm crys}(\mathbf{r})$ and $\rho_{\rm NL}^{\rm crys}(\mathbf{r})$, one can use an integration scheme appropriate to each piece. Our basic goal is to isolate in $\rho_{\rm L}^{\rm crys}(\mathbf{r})$ the density peaks arising (largely) from the core states, and to keep $\rho_{\rm NL}^{\rm crys}(\mathbf{r})$ as slowly varying as possible. We start by defining $\rho_{\rm L}^{\rm crys}(\mathbf{r})$ to be a lattice superposition of nonoverlapping, atom-centered terms:

$$\rho_{\rm L}^{\rm crys}(\mathbf{r})=\sum_{\gamma\nu}\rho_{\rm L}^{\gamma}(\mathbf{r}-\mathbf{R}_\nu-\mathbf{T}_\gamma)\ . \quad (5)$$

Each localized function $\rho_{\rm L}^{\gamma}(\mathbf{r})$ is constructed according to the following scheme. For convenience, we (temporarily) define the coordinate origin to be at $\mathbf{R}_\nu+\mathbf{T}_\gamma$, the relevant atomic site. A cutoff radius $R_{\rm cut}$ is chosen (we temporarily omit the γ superscript), outside of which $\rho_{\rm L}(\mathbf{r})$ will be identically zero. (This parameter is typically chosen to be roughly one-fourth the nearest-neighbor distance, so that the resulting spheres are well separated.) Inside the sphere, the electronic part of $\rho^{\rm crys}(\mathbf{r})$ is well approximated by a lattice harmonic expansion of the form

$$\rho_{\rm LH}(\mathbf{r})=\sum_l \rho_l(r)X_l(\hat{\mathbf{r}})\ , \quad (6)$$

in which the $\rho_l(r)$ are numerical functions and the $X_l(\hat{\mathbf{r}})$ are lattice harmonics, i.e., solutions to the Laplace equation that are invariant under the operations of the local

point group. Efficient angular meshes, giving $\hat{\mathbf{r}}$ directions and corresponding volume elements (weighting factors), are used to guarantee that all lattice harmonics up to a fixed value of l integrate correctly over the unit sphere.[10] Moreover, in contrast to the LAPW method, it is not necessary to include a large number of terms in this expansion, as any difference between $\rho_{\rm L}(\mathbf{r})$ and $\rho_{\rm LH}(\mathbf{r})$ will be absorbed by the nonlocalized term $\rho_{\rm NL}^{\rm crys}(\mathbf{r})$. A second lattice harmonic expansion, $\eta_{\rm LH}(\mathbf{r})=\sum_l \eta_l(r)X_l(\hat{\mathbf{r}})$, is now defined for the same l values that appear in Eq. (6), in order to smoothly extend the charge density *outside* the sphere to the interior. This is done by choosing the functions $\eta_l(r)$ to have the form $\eta_l(r)=\alpha_l r^p \exp(-\beta_l r)$, where $p=0$ for $l=0$ and $p=1$ for $l>0$, and the two parameters α_l and β_l are chosen so that the values and first derivatives of $\rho_l(r)$ and $\eta_l(r)$ match at the sphere boundary. Now we may define the localized function $\rho_{\rm L}(\mathbf{r})$ according to

$$\rho_{\rm L}(\mathbf{r})=\begin{cases}\rho_{\rm LH}(\mathbf{r})-\eta_{\rm LH}(\mathbf{r}) & \text{for } r\le R_{\rm cut}\\ 0 & \text{for } r>R_{\rm cut}\ .\end{cases} \tag{7}$$

With this definition, it is clear that $\rho_{\rm L}(\mathbf{r})$ goes smoothly to zero at the sphere boundary. Equations (5) and (7) now determine the entire localized contribution, $\rho_{\rm L}^{\rm crys}(\mathbf{r})$, to the total crystal charge density. Since the nuclear charge is uniquely defined, the nonlocalized contribution is now simply defined as the charge not yet accounted for:

$$\rho_{\rm NL}^{\rm crys}(\mathbf{r})=\rho^{\rm crys}(\mathbf{r})-\rho_{\rm L}^{\rm crys}(\mathbf{r})-\rho_{\rm nuc}^{\rm crys}(\mathbf{r})\ . \tag{8}$$

With the decomposition of the density now specified, we turn to the resulting Coulomb potential. Two problems arise here. First, although the potential arising from $\rho^{\rm crys}(\mathbf{r})$ is everywhere finite (except at the atomic centers), the three contributions arising from Eq. (4) are separately divergent, due to the infinite lattice summation of terms whose long-range behavior is $|\mathbf{r}-\mathbf{R}_\nu|^{-1}$. Second, although the localized density that we have defined can be accurately integrated on a dense (one-dimensional) radial mesh, the nonlocalized density has a cusp at every atomic site, arising from the peaked function $\eta_0(r)$. The two problems have a single solution. By adding [to $\rho_{\rm L}^{\rm crys}(\mathbf{r})$] and subtracting [from $\rho_{\rm NL}^{\rm crys}(\mathbf{r})$] a function, $\xi^{\rm crys}(\mathbf{r})$, the decomposition of the density finally takes the form

$$\begin{aligned}\rho^{\rm crys}(\mathbf{r})=&[\rho_{\rm L}^{\rm crys}(\mathbf{r})+\rho_{\rm nuc}^{\rm crys}(\mathbf{r})+\xi^{\rm crys}(\mathbf{r})]\\ &+[\rho_{\rm NL}^{\rm crys}(\mathbf{r})-\xi^{\rm crys}(\mathbf{r})]\ .\end{aligned} \tag{9}$$

The function $\xi^{\rm crys}(\mathbf{r})$ is chosen to be a lattice superposition of exponential functions,

$$\xi^{\rm crys}(\mathbf{r})=\sum_{\gamma\nu}\xi^{\gamma}(\mathbf{r}-\mathbf{R}_\nu-\mathbf{T}_\gamma)\ ,$$

$$\text{with } \xi^{\gamma}(\mathbf{r})=a_\gamma\exp(-b_\gamma r)\ , \tag{10}$$

so that there are two adjustable parameters, a_γ and b_γ, for each inequivalent atom in the unit cell. These parameters are chosen so that (i) each bracketed term in Eq. (9) gives zero when integrated over any unit cell, and (ii) the cusps at each atomic site in $\rho_{\rm NL}^{\rm crys}(\mathbf{r})$ are explicitly subtracted off.

The calculation of the Coulomb potential $V_{\rm Coul}(\mathbf{r})$ is now quite simple, and has two contributions. The first, arising from the first bracketed term in Eq. (9), is a lattice summation of potentials from uncharged spheres and hence converges at least as fast as $|\mathbf{r}-\mathbf{R}_\nu|^{-2}$. The mesh most appropriate to this localized density (and potential) is radially exponential, allowing the required numerical integrations to be done accurately by a one-dimensional cubic spline algorithm. The second bracketed density term extends over the whole unit cell, is charge neutral, and is slowly varying. It is evaluated on a mesh of points of the form

$$\mathbf{r}(n_1,n_2,n_3)\equiv(n_1/N_1)\mathbf{a}_1+(n_2/N_2)\mathbf{a}_2+(n_3/N_3)\mathbf{a}_3\ ,$$

$$0\le n_i<N_i\ , \tag{11}$$

where the $\mathbf{a}_i$ are the primitive lattice vectors. The calculation of the resulting potential is then performed in reciprocal space by a fast Fourier transform algorithm. Finally, the contribution from this component of the potential to the radial mesh points inside the spheres is calculated by linear tetrahedral interpolation.

In some cases, the above procedure may be slightly altered. For strongly ionic crystals (e.g., the alkali halides and II-VI compounds) it is customary to decompose the nuclear charge Z_γ according to the ionicity I_γ of atom γ, i.e., $Z_\gamma=(Z_\gamma-I_\gamma)+I_\gamma$, where I_γ is taken as positive for a cation. The calculation of the Coulomb potential then proceeds as before, with the nuclear charge of atom γ redefined as $Z_\gamma-I_\gamma$. The final contribution to the Coulomb potential is the Madelung potential formed by the point charges I_γ. This procedure, which has been successfully used for a variety of alkali halide crystals,[11,12] has two advantages. First, the Coulomb potential for neutral atoms converges more rapidly than for ions, while efficient numerical techniques can be used for calculating the Madelung potential. Second, the LCAO Gaussian basis sets can be taken from free ion (rather than free atom) calculations, so that the ionic crystal is already well described at the zeroth iteration by the overlapping (ionic) charge density.

A simple test of the quality of our density decomposition is to numerically integrate the total electronic charge on the mesh described above. We have done this test using the fully self-consistent charge density for diamond, which is highly directional due to strong covalent bonding. For a mesh of 477 inequivalent points in the Wigner-Seitz cell, the total electronic charge density integrates to 11.998 electrons. By increasing the number of mesh points to 1365, the density integrates to 11.99998, i.e., by tripling the number of mesh points, the error is reduced by 2 orders of magnitude.

Finally, the electronic charge density itself is calculated directly from the eigenvectors $\psi_n(\mathbf{k},\mathbf{r})$ of the Hamiltonian defined by $V_{\rm eff}(\mathbf{r})$, thus providing the link between input and output potentials in the self-consistency cycle. This may be written as

$$\rho(\mathbf{r})=\sum_{n,\mathbf{k}} w(\mathbf{k})|\psi_n(\mathbf{k},\mathbf{r})|^2 f(E_n(\mathbf{k})-E_F)\ , \tag{12}$$

where $w(\mathbf{k})$ is a Brillouin-zone weight, $f(E)$ is the

Fermi-Dirac distribution function, and E_F is the Fermi energy as determined by charge conservation. As is the usual practice for self-consistent calculations, we accelerate convergence by using as input to the next iteration a weighted average of the current and previous iterations, as determined by the modified Broyden's method.[13]

III. RESULTS AND DISCUSSION

A. Diamond

The electronic properties of cubic diamond have been thoroughly investigated by a large number of workers, both theoretical[14–24] and experimental.[25] We have chosen diamond as a first test case partially for this reason, and partially because we are in the process of applying LCAO techniques to a wide variety of diamond-related materials (e.g., surfaces,[26] interfaces,[5,6] and clusters[27]). Furthermore, the highly directional sp^3 bonding in diamond tests the ability of any computational scheme to accurately represent large deviations from overlapping spherical densities. Finally, diamond is the prototypical covalently bonded insulator, and as such has become a standard test case for electronic-structure calculations; this gives us ample theoretical results with which to compare our method.

We have performed parallel LCAO and LAPW calculations on bulk diamond, using the LCAO method described in Sec. II, and the LAPW bulk codes of Krakauer and collaborators.[4] The experimental lattice constant of 6.741 a.u. was used, and both calculations used the Hedin-Lundqvist[28] form of the exchange-correlation potential. Both calculations were iterated to self-consistency using ten special **k** points in an irreducible wedge of the Brillouin zone. To compute the density of states (DOS), the Hamiltonian was diagonalized at 280 **k** points in the irreducible zone. Fourier interpolation to a much denser mesh[29] and the linear tetrahedron method were then used to generate the DOS curves that appear in Fig. 1.

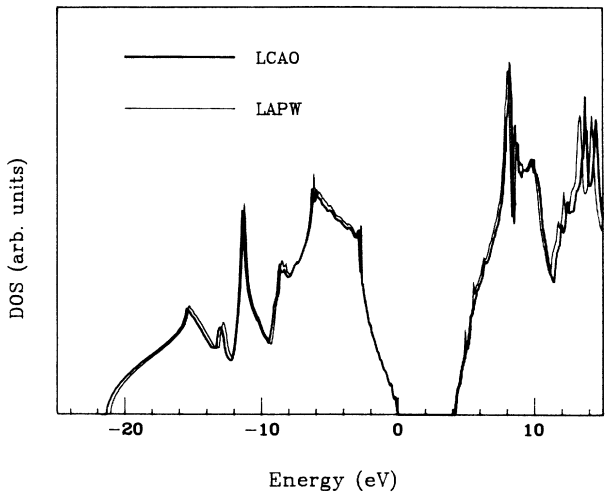

FIG. 1. Total density of states (DOS) for the valence and lower conduction bands of bulk diamond. The thick curve is the LCAO result, and the thin curve is the LAPW result.

The LCAO basis set consisted of six s-type, five p-type, and one d-type Gaussian orbitals, denoted as C(6/5/1), for a total of 54 functions per two-atom cell. The single cutoff radius was set at $R_{cut}=0.75$ a.u., so that the atomic spheres accounted for only 4.7% of the primitive cell volume. With such small spheres, it is reasonable to include only the $l=0$ term in Eq. (6). We used six radial directions in order to pick out this $l=0$ component, with 51 mesh points in each direction, and an interstitial mesh of 204 points in the fundamental real-space wedge. The total number of inequivalent mesh points was thus 510, which enables the electronic charge to be integrated numerically to 11.998 electrons. While it is certainly possible to reduce this error considerably (see the end of Sec. II), we will see that this is apparently not necessary for the accurate calculation of eigenvalue spectra. Indeed the excellent agreement between the LAPW and LCAO results (see below) indicates that our Coulomb potential algorithm is reasonably robust, in the sense that a fairly small number of points gives a sufficiently accurate solution to the Poisson equation. Of course for calculations that depend more sensitively on the details of the potential, such as total energy differences, this level of accuracy may not be sufficient, and significantly more mesh points may be required.

The LAPW method has been described in detail elsewhere,[4] so we include here only the relevant numerical details. The atomic sphere radius was 1.419 a.u., and the charge density and potential were expanded inside these spheres up to $l=8$. The RK_{max} value was taken as 7.5, resulting in a basis set consisting of approximately 175 functions.

The resulting DOS curves appear in Fig. 1, for both the LCAO and LAPW methods. Clearly, the agreement is excellent, throughout not only the wide valence band, but also in the lowest 12 eV or so of the conduction-band region. We do note a slight (0.2 eV) upward shift of the LCAO DOS, relative to the LAPW DOS, in the upper conduction band. A similar downward shift occurs in the lower valence region.

There have been many self-consistent calculations of the diamond band structure, using both reciprocal-space methods[18,22] and real-space methods.[14–17,19–21,23,24] In Table I, we have tabulated a number of valence and conduction levels computed by our (full-potential) parallel LCAO and LAPW calculations, a pseudopotential plane-wave (PS-PW) calculation[22], a pseudopotential Gaussian-orbital (PS-GO) calculation[20], and a pseudopotential LCAO (PS-LCAO) calculation[21]. The first three calculations (LCAO, LAPW and the PS-PW calculation of Pickett and Wang,[22] i.e., the first three columns of Table I) all used the experimental diamond lattice constant and the Hedin-Lundqvist exchange-correlation potential. Furthermore, all three calculations used basis sets large enough to give well-converged eigenvalue spectra: 54 local functions for LCAO, 175 PW's for LAPW, and 300 PW's for PS-PW. The agreement among these three calculations is very good, with typical discrepancies in the range of one- or two-tenths of an eV. Agreement with the last two columns of Table I is also good, although somewhat less so. Of course, differences in the

TABLE I. Diamond energy levels (in units of eV) at the Γ, X, and L points, as calculated by several different methods. Notation is as follows: LCAO and LAPW (the present calculations), PS-PW (pseudopotential plane wave, Ref. 22), PS-GO (pseudopotential Gaussian orbital, Ref. 20), PS-LCAO (pseudopotential LCAO, Ref. 21).

Root	LCAO	LAPW	PS-PW	PS-GO	PS-LCAO
Γ_1	−21.34	−21.06	−21.38	−21.68	−21.03
$\Gamma_{25'}$	0	0	0	0	0
Γ_{15}	5.57	5.51	5.51	5.59	6.02
$\Gamma_{2'}$	13.56	13.13	13.56	13.07	13.41
X_1	−12.66	−12.48	−12.67	−12.90	−12.43
X_4	−6.34	−6.18	−6.31	−6.43	−6.27
X_1	4.79	4.68	4.64	4.65	5.91
X_4	16.71	16.41	16.81	16.87	16.77
$L_{2'}$	−15.52	−15.33	−15.53	−15.79	−15.29
L_1	−13.41	−13.14	−13.47	−13.73	−13.09
$L_{3'}$	−2.81	−2.73	−2.81	−2.86	−2.82
L_3	8.45	8.33	8.37	8.47	9.23
L_1	9.07	8.75	8.97	8.90	9.58

detailed spectra can to some extent be attributed to different assumptions and objectives. The PS-LCAO calculation of Chelikowsky and Louie[21] used a lattice constant of $a=6.727$ a.u. (computed from total energy minimization), slightly smaller than our value, and a small basis set consisting of 24 functions. However, their objective was not the accurate calculation of virtual levels, but rather than prediction of ground state structural properties and cohesive energies. Indeed, the most serious disagreement between their LCAO eigenvalue spectrum and ours occurs in the higher conduction-band states at the edge of the zone, which is not surprising in light of their smaller basis set. The pseudopotential Gaussian-orbital calculation of Bachelet *et al.*[20] was performed using Wigner correlation and a predicted lattice constant of 6.97 a.u. (3% larger than our value). The good agreement with our eigenvalues is somewhat surprising, especially since Zunger and Freeman have shown[16] that the one-electron energies in diamond vary rather strongly with lattice constant, with the conduction levels falling and the valence levels rising as the lattice expands. No such compression is observed in the levels of Bachelet *et al.*,[20] and so we can only surmise that this effect is offset to some degree by the different choice of correlation functional.

Diamond is unusual among covalently bonded solids in that the self-consistent valence charge density shows a double-humped structure along the bonding chains, with peaks located from $\frac{1}{2}$ to $\frac{2}{3}$ of the distance to the bond center. The presence of these peaks is a good test of a method's ability to represent large deviations from overlapping spherical densities, since the peaks are absent in a plot of the overlapping atomic valence density. In Fig. 2(a), we show the LCAO self-consistent diamond valence density along one of the bonding chains, computed from ten special **k** points; the corresponding result for the LAPW calculation appears in Fig. 2(b). In both, the double humps are evident, with the peaks occurring on the bond axis at a distance 0.77 a.u. from the atomic center, quite similar to the results of Bachelet *et al.*[20] The LCAO bond charge maximum of 0.28 a.u. is also in good agreement with the result of 0.30 a.u. found by Bachelet *et al.*,[20] and agrees with our LAPW result to within 1.5%. Furthermore, the overall agreement between the LCAO and LAPW results is clearly very good as well. The only significant differences evident from Fig. 2 are (i) a slight discrepancy in the bond charge maximum, and (2) greater evidence of back-bonding lobes in the LAPW result. This latter is probably the result of having many more radial mesh points near the atomic cores in the LAPW calculation.

B. Vanadium

Although we use the same method as for insulators, the calculation for a metal is potentially more sensitive to numerical details. For a transition metal such as vanadium, the *d* bands give rise to a substantial charge density in the interstitial regions of the cell, making accurate representation of the density and potential away from the cores of particular importance. Furthermore, the sharp peak in the DOS near the Fermi energy, which is characteristic of the transition metals, makes the self-consistent band structure particularly sensitive to the detailed shape of the potential. For these reasons, both the LCAO and LAPW calculations were iterated to self-consistency using a relatively large set of 44 special **k** points in the irreducible zone. For the DOS calculation, diagonalizations were performed at 256 inequivalent points, followed by Fourier interpolation to a denser mesh.

Vanadium has the bcc structure, and we have used the experimental value of 5.698 a.u. for the lattice constant. The LCAO basis set was V(7/5/3), so that the total number of basis functions was 40. The cutoff radius was $R_{\rm cut}=1.35$ a.u., so that the sphere volume accounted for 11% of the total cell volume. Because of the octahedral site symmetry, only three independent directions were

needed to pick out the $l=0$ component of the density. Each direction used 112 radial mesh points, and the fundamental wedge contained 120 interstitial mesh points. With these 456 inequivalent points, the charge density numerically integrated to 22.9996 electrons.

For the LAPW calculation, the atomic sphere radius was 2.250 a.u., and lattice harmonics inside the sphere were taken up to $l=8$. The $RK_{\max}$ value was 9.5, which resulted in a total of approximately 115 basis functions.

In Table II we have tabulated a number of the resulting vanadium energy levels around the Fermi energy, at several high-symmetry points in the bcc Brillouin zone. The agreement is excellent near the Fermi level (less than 0.1 eV difference between the LCAO and LAPW results), and somewhat less good near the bottom and top of this energy range.

TABLE II. Vanadium energy levels (in units of eV) at the Γ, H, and P points in the bcc Brillouin zone, as calculated by the LCAO and LAPW methods. The Fermi level is taken as the zero of energy in each case.

Root	LCAO	LAPW
Γ_1	−6.27	−6.45
$\Gamma_{25'}$	0.37	0.39
Γ_{12}	2.32	2.35
H_{12}	−2.94	−2.91
$H_{25'}$	3.61	3.67
H_{15}	10.44	10.08
P_4	−1.07	−1.07
P_3	2.73	2.76
P_4	10.46	10.48

The DOS for the d bands near the Fermi level appears in Fig. 3, for both the LCAO and LAPW methods. The agreement is excellent throughout the 15-eV region shown. All of the major features are very nearly coincident, and many of the minor features (shoulders and humps) are reproduced by both methods as well. We note also that no adjustment of the Fermi level or overall scaling was performed to bring the two curves into better agreement, i.e., the LCAO and LAPW Fermi levels were each determined self-consistently.

In Figs. 4(a) and 4(b), we show the valence charge density as calculated by the LCAO and LAPW methods, respectively. Vanadium has five valence electrons, which in the solid occupy states of e_g and t_{2g} character. A predominance of the latter give rise to the distinctive

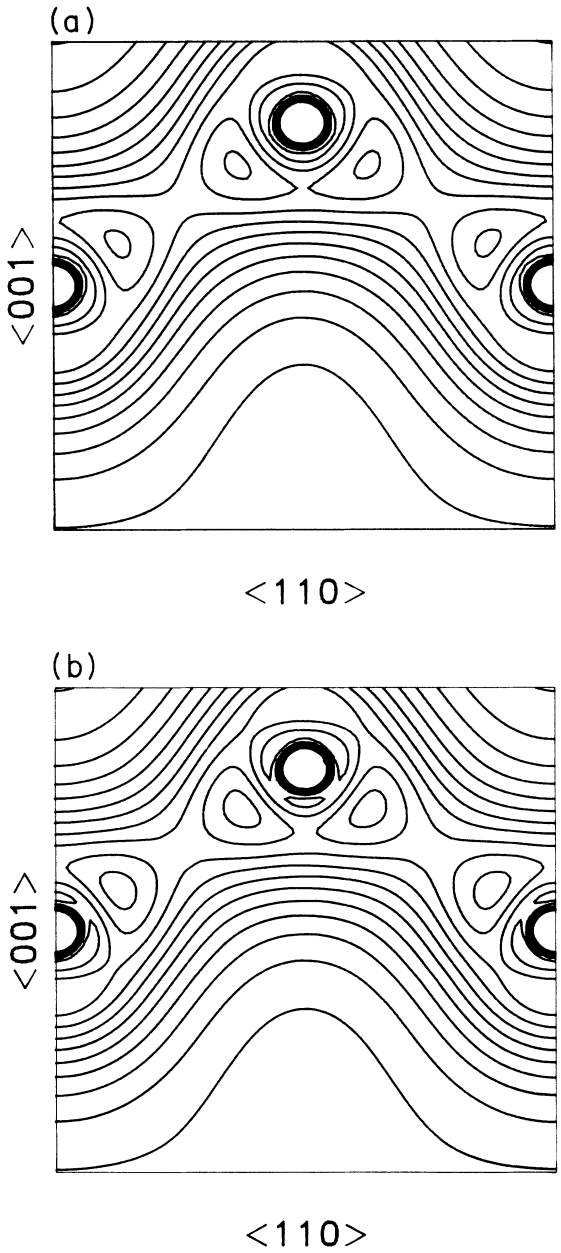

FIG. 2. Valence charge density in bulk diamond, along a bonding chain, calculated with (a) the LCAO method, and (b) the LAPW method. Note the double peaks along each bonding axis. The contour spacing is 0.025 a.u., which is also the value of the lowest contour.

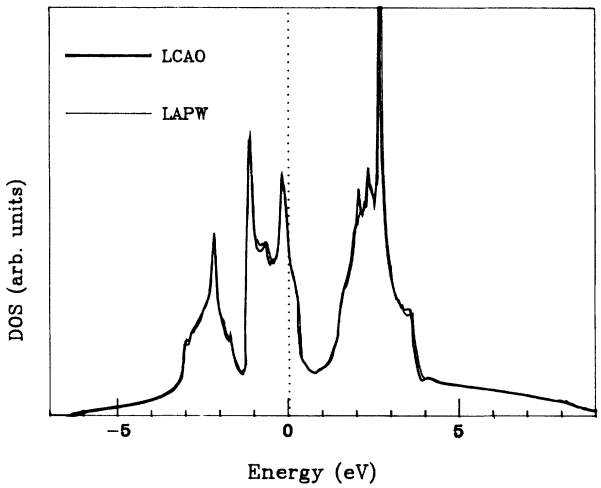

FIG. 3. Total density of states (DOS) for bulk bcc vanadium. The thick and thin lines are the LCAO and LAPW results, respectively. The Fermi energy has been set to zero in each case.

kidney-shaped double lobes close to the atomic core, while an *s*-like contribution accounts for the more nearly spherical distribution away from the core. The overall agreement between the two densities is clear. As was the case in diamond, the LAPW calculation again shows slightly more structure around the core region, probably the result of greater sampling in that region. We also note a slight difference in the size and shape of the lowest (interstitial) contour.

C. Diamond-nickel (001) interface

For our last comparison between the LCAO and LAPW methods, we turn to a significantly larger unit cell with much lower site symmetry. The ideal diamond-nickel (001) interface has been studied theoretically in separate publications,[5,6] to which we refer the reader for a more detailed discussion than is appropriate here. Briefly, we have modeled the interface with a supercell consisting of four-layer C slabs alternating with three-layer Ni slabs. Bulk diamond and nickel are lattice matched to within 1.5%, and we have ignored the remaining mismatch and strain by using the bulk nickel lattice constant ($a=6.644$ a.u.) for both the diamond and nickel slabs. The seven-atom unit cell (see Fig. 5) is generated by first positioning the four C atoms at their diamond lattice sites (four layers), then positioning a Ni atom in the fifth layer at the position that would have been occupied by a C atom in bulk diamond. The remaining two Ni atoms are positioned relative to the first according to the bulk nickel fcc geometry. This construction results in a C-Ni spacing that is unrealistically small, and so we separate the diamond and Ni slabs by an amount that gives a C-Ni spacing of 3.55 a.u., roughly midway between the C-C and Ni-Ni spacing. This unit cell has inversion symmetry about the midpoint of the two-central C atoms, so that there are only four inequivalent atoms: interior and interface C, and interior and interface Ni.

For the LCAO calculation, the basis set was chosen to be C(6/5/0) and Ni (7/5/3) for carbon and nickel, respectively, for a total basis set size of 204. Since C *d*-type basis functions were found to be unnecessary in the bulk diamond calculation, we have omitted them here in the interest of a smaller basis set. The C cutoff radius was 0.56 a.u., the interface Ni cutoff was 1.39 a.u., and the central Ni cutoff was 1.57 a.u., resulting in a total atomic sphere volume that was 11% of the primitive cell volume. With a total of 4318 inequivalent mesh points, the total charge density integrated to 107.998 electrons. Note that relative to diamond, scaling the total number of mesh points with the total number of electrons holds the integration error constant.

For the LAPW calculation, the C and Ni sphere radii were taken as 1.419 and 2.000 a.u., respectively. The C

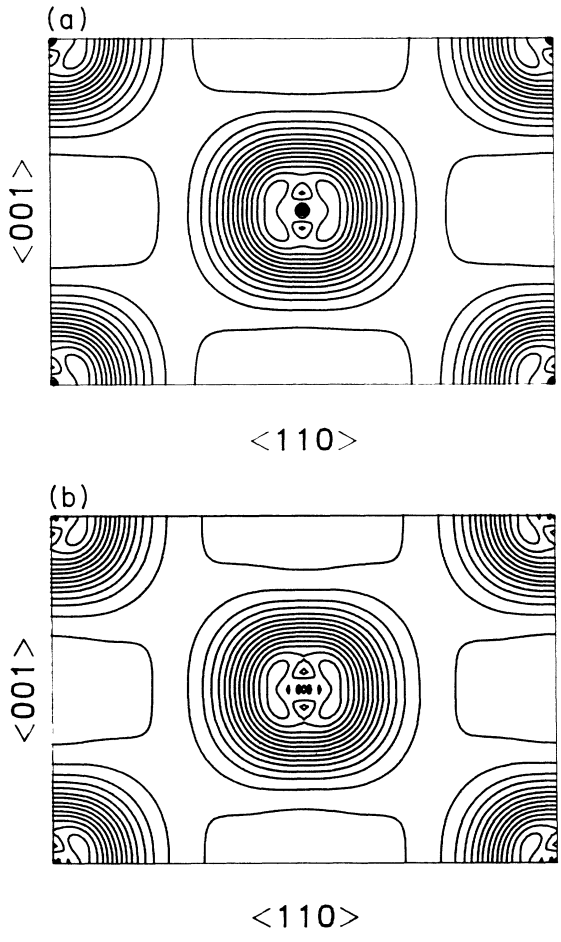

FIG. 4. Valence charge density for vanadium in a (110) plane, as calculated by (a) the LCAO method, and (b) the LAPW method. The kidney-shaped lobes arise from a small predominance of $3d(t_{2g})$ component. The smallest (interstitial) contour has the value 0.04 a.u., and the kidney-shaped contour has the value 0.39 a.u. Adjacent contours differ by 20%.

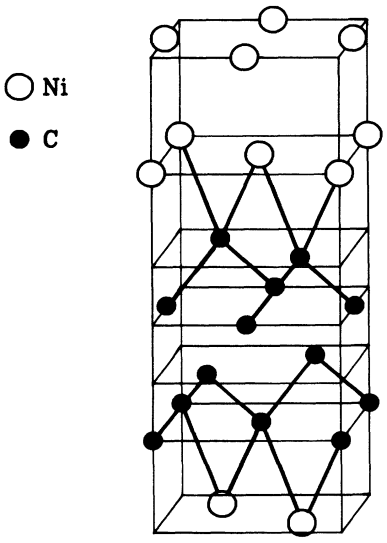

FIG. 5. Supercell geometry for the ideal diamond-nickel (001) interface. Fourfold coordination of interface C atoms is indicated by heavy lines. Note that there are only four inequivalent atoms: interior and interface C, and interior and interface Ni.

1s and Ni 1s, 2s, 2p, 3s, and 3p states were treated as core states with a fully relativistic Hamiltonian, and all remaining C and Ni states were treated as scalar-relativistic valence-band states. (We note that although the LCAO calculation was nonrelativistic, the inclusion of relativistic terms in the LAPW calculation serves mainly to shift the levels of the core states, without significantly affecting the chemistry of the valence states.) The C and Ni RK_{max} values were 6.0 and 8.4, respectively, which led to a basis-set size of approximately 520.

For both the LCAO and LAPW calculations, the charge density was iterated to self-consistency using nine special **k** points in the irreducible zone. Direct diagonalization at 75 inequivalent **k** points, followed by the usual Fourier interpolation, produced the DOS curves. To generate the local densities of states (LDOS) for the four inequivalent atoms, a standard Mulliken projection technique[30] was used for the LCAO method, and a charge-within-spheres projection was used for the LAPW method. The DOS and projected LDOS for both methods appear in Fig. 6 (reproduced from Ref. 5). In this figure, the Ni-projected LDOS have all been divided by a factor of 10 with respect to the C LDOS, for clarity of display. Despite the fact that two different projection techniques were used to decompose the total DOS, all five panels in Fig. 6 show remarkable agreement. A number of features are noteworthy. The lower C valence band, from -20 to -10 eV, shows a slab structure characteristic of size quantization induced by the supercell, which is apparently too small to represent bulk diamond accurately. The interior Ni atoms, however, are well screened and show a LDOS quite similar to that seen in the bulk, with a characteristic two-peaked structure and large peak at the Fermi level. In the low-energy tails a small supercell effect is evident. Finally, a large interface density of states appears on the interfacial C atom, derived from a nonbonding combination of C p_x and p_y and Ni d_{xz} and d_{yz} states. All of these structures, discussed in greater detail in Refs. 5 and 6, are accurately reproduced in both the LCAO and LAPW results.

Differences between the two methods are seen primarily in the presence or absence of very sharp spikes in the DOS and LDOS. These are artifacts of the Fourier interpolation scheme, and are generally not related to the eigenvalue spectrum. In the region 2–5 eV above the Fermi level, there are some small but real differences in the total DOS given by the two methods. By close examination of the projected LDOS in this energy range, it is clear that most of these differences arise from the interface Ni atom (recall the factor of 10 difference in scale relative to C). Given the isolated nature of the differences, as well as their small scale relative to the occupied DOS, we feel them to be relatively unimportant.

We offer a further comparison of the LCAO and LAPW results in Table III. For this diamond-nickel supercell, the inequivalence of the interior and interface

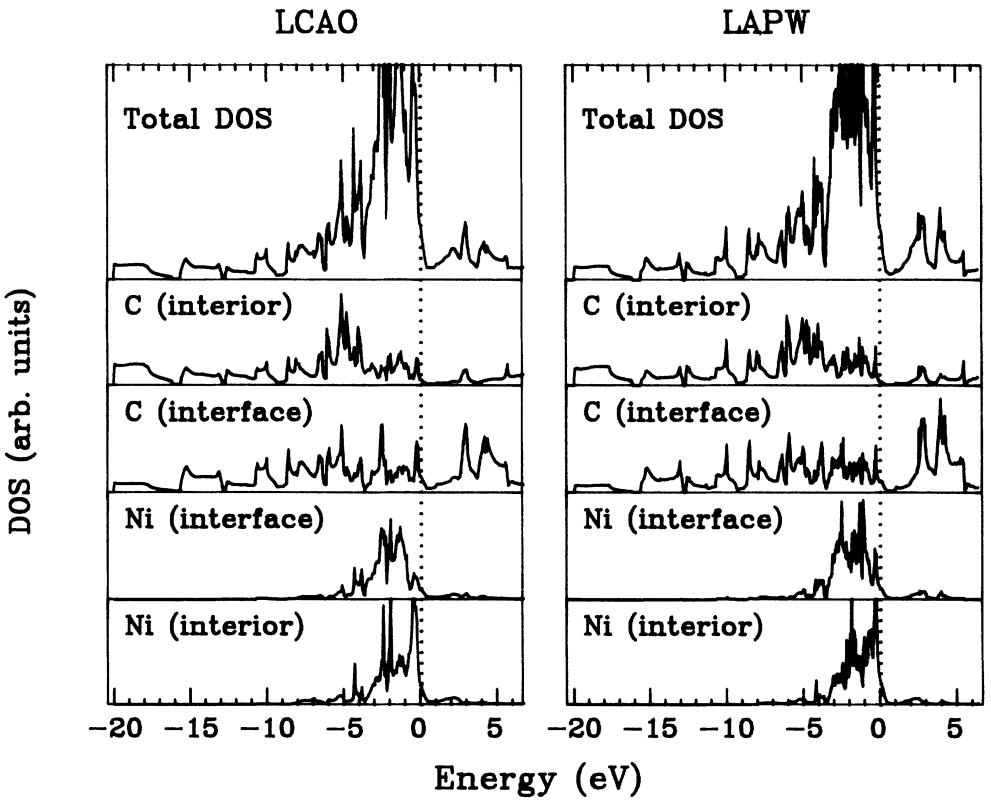

FIG. 6. Total and local density of states (DOS) for the diamond-nickel interface supercell (described in the text), as calculated by the LCAO (left) and LAPW (right) methods. The local DOS for the two nickel atoms has been divided by a factor of 10 relative to carbon, for display purposes. For the LCAO result, the local DOS is projected by a Mulliken decomposition, while for the LAPW result a charge-within-spheres technique is used.

TABLE III. Core state energy level differences (in units of eV) for the diamond-nickel interface supercell. $\Delta\varepsilon$(Ni) is the difference between core state eigenvalues associated with the two inequivalent Ni atoms; similarly for $\Delta\varepsilon$(C) (see the last paragraph of Sec. III C for further discussion).

	1s		2s		3s	
	LAPW	LCAO	LAPW	LCAO	LAPW	LCAO
$\Delta\varepsilon$(Ni)	0.58	0.46	0.71	0.73	0.60	0.57
$\Delta\varepsilon$(C)	0.15	0.05				

atoms gives rise to a small energy difference between the deep (dispersionless) core levels for, say, the 1s states of the interior and interface Ni atoms. Although the inclusion of relativistic corrections in the LAPW method gives *absolute* core level energies quite different from the nonrelativistic LCAO method, this energy *difference* should be directly comparable. Hence, in Table III we tabulate the quantities

$$\Delta\varepsilon(\text{Ni}) \equiv \varepsilon(\text{interior Ni}) - \varepsilon(\text{interface Ni}) \quad (13)$$

and

$$\Delta\varepsilon(\text{C}) \equiv \varepsilon(\text{interior C}) - \varepsilon(\text{interface C}) , \quad (14)$$

where ε denotes an eigenvalue for the states listed in the table. Although the absolute energy levels themselves span a very large range, from roughly -300 a.u. (the Ni 1s state) to roughly -3 a.u. (the Ni 3s state), the energy splittings $\Delta\varepsilon$(Ni) given by the LAPW and LCAO methods are in remarkable agreement. The three splittings shown for Ni are of order 1 eV, and the agreement between the LAPW and LCAO splittings is approximately 0.1 eV or better. For the single C core level, the splitting itself is of order 0.1 eV, and the discrepancy between LAPW and LCAO is also 0.1 eV.

IV. SUMMARY

We have described a new first-principles, general-potential method for calculating electronic band structure using a LCAO basis set and Gaussian-type orbitals. By performing parallel LCAO and LAPW calculations on diamond, vanadium, and the diamond-nickel (001) ideal interface, we have shown that this method is capable of accuracy quite comparable to the LAPW method for the systems studied so far. It is important to note that in these tests, neither the LCAO nor the LAPW basis sets have been reduced to the most efficient sets that still give accurate results. Indeed, the convergence criteria for the LAPW calculations have been set abnormally high, in order to provide stringent tests of our new LCAO method. In future studies, we plan to investigate optimization of the LCAO basis sets, and to determine the actual scaling of the LCAO computing time requirement as a function of the number of basis functions per unit cell.

ACKNOWLEDGMENTS

We are grateful for numerous discussions with H. Krakauer, D. Singh, and K. A. Jackson, as well as for generous contributions of computer code by D. Singh and D. D. Johnson. One of us (S.E.) acknowledges generous financial support from the National Research Council. This work was supported in part by the Innovative Science and Technology Program of the Strategic Defense Initiative Organization, Contract N00014-90-WX-24138, through the U.S. Office of Naval Research. The majority of calculations was performed on the IBM 3090 supercomputer at the Cornell National Supercomputing Facility, and on the Cray Research, Inc. X-MP/24 supercomputer at the Naval Research Laboratory.

[1]W. E. Pickett, in *Supercomputing '88: Supercomputing Projects, Applications and Artificial Intelligence,* edited by L. P. Kartashev and S. I. Kartashev (International Supercomputing Institute, Inc., St. Petersburg, Florida, 1988), p. 172.

[2]R. Car and M. Parrinello, Phys. Rev. Lett. **55**, 2471 (1985); Solid State Commun. **62**, 403 (1987).

[3]O. K. Andersen, Phys. Rev. B **12**, 3060 (1975).

[4]E. Wimmer, H. Krakauer, M. Weinert, and A. J. Freeman, Phys. Rev. B **24**, 864 (1981); D. R. Hamann, Phys. Rev. Lett. **42**, 662 (1979); S.-H. Wei and H. Krakauer, *ibid.* **55**, 1200 (1985); S.-H. Wei, H. Krakauer, and M. Weinert, Phys. Rev. B **32**, 7792 (1985).

[5]W. E. Pickett and S. C. Erwin, Phys. Rev. B **41**, 9756 (1990).

[6]W. E. Pickett and S. C. Erwin, in *Wide-Bandgap Semiconductors,* edited by J. T. Glass, R. F. Meissier, and N. Fujimori (Materials Research Society, Pittsburgh, 1990).

[7]For a comprehensive review of the LCAO and other methods, see D. D. Koelling, Rep. Prog. Phys. **44**, 139 (1981). An early paper on Gaussian-orbital methods is R. C. Chaney, T. K. Tung, C. C. Lin, and E. E. Lafon, J. Chem. Phys. **52**, 361 (1970).

[8]W. Y. Ching, C. C. Lin, and D. L. Huber, Phys. Rev. B **14**, 620 (1976).

[9]W. H. Press, B. P. Flannery, S. A. Teukolsky, and W. T. Vetterling, *Numerical Recipes: The Art of Scientific Computing* (Cambridge University Press, Cambridge, England, 1988).

[10]A. H. Stroud, *Approximate Calculations of Multiple Integrals* (Prentice-Hall, Englewood Cliffs, NJ, 1971).

[11]S. C. Erwin, R. A. Heaton, and C. C. Lin, *BandAid: A Software Package for the Calculation of Electronic Band Structure by the LCAO Method* (University of Wisconsin Board of Regents, 1986).

[12]S. C. Erwin and C. C. Lin, J. Phys. C **21**, 4285 (1988).

[13]C. G. Broyden, Math. Comput. **19**, 577 (1965); D. D. Johnson, Phys. Rev. B **38**, 12 807 (1988).

[14]R. C. Chaney, C. C. Lin, and E. E. Lafon, Phys. Rev. B **3**, 459 (1971).

[15]G. S. Painter, D. E. Ellis, and A. R. Lubinsky, Phys. Rev. B **4**, 3610 (1971).

[16]A. Zunger and A. J. Freeman, Phys. Rev. B **15**, 5049 (1977).

[17]R. A. Heaton and E. E. Lafon, Phys. Rev. B **17**, 1958 (1978).
[18]M. T. Yin and M. L. Cohen, Phys. Rev. B **24**, 6121 (1981); Phys. Rev. Lett. **50**, 2006 (1983), and references therein.
[19]D. Glötzel, B. Segall, and O. K. Andersen, Solid State Commun. **36**, 403 (1980).
[20]G. B. Bachelet, H. S. Greenside, G. A. Baraff, and M. Schlüter, Phys. Rev. B **24**, 4745 (1981).
[21]J. R. Chelikowsky and S. G. Louie, Phys. Rev. B **29**, 3470 (1984).
[22]W. E. Pickett and C. S. Wang, Phys. Rev. B **30**, 4719 (1984).
[23]B. Holland, H. S. Greenside, and M. Schlüter, Phys. Status Solidi B **126**, 511 (1984).
[24]W. R. L. Lambrecht and O. K. Andersen, Phys. Rev. B **34**, 2439 (1986).
[25]*The Properties of Diamond,* edited by J. E. Field (Academic, London, 1979).
[26]M. R. Pederson, K. A. Jackson, and W. E. Pickett, in *Technology Update on Diamond Films,* edited by R. P. H. Chang, D. Nelson, and A. Hiraki (Materials Research Society, Pittsburgh, 1989).
[27]K. A. Jackson, M. R. Pederson, and J. G. Harrison (unpublished).
[28]L. Hedin and B. I. Lundqvist, J. Phys. C **4**, 2064 (1971).
[29]W. E. Pickett, H. Krakauer, and P. B. Allen, Phys. Rev. B **38**, 2721 (1988).
[30]R. S. Mulliken, J. Chem. Phys. **23**, 1833 (1955).